



Biomechanical and Clinical Study of Rod Curvature in Single-Segment Posterior Lumbar Interbody Fusion

Lin Han^{1†}, Yongheng Li^{2†}, Zhiyong Li^{2,3}, Hongdao Ma¹, Chenfeng Wang¹, Qiang Chen^{2*} and Xuhua Lu^{1*}

¹Department of Orthopaedics, Shanghai Changzheng Hospital, Second Military Medical University, Shanghai, China,

²Biomechanics Laboratory, School of Biological Science and Medical Engineering, Southeast University, Nanjing, China, ³School of Mechanical Medical and Process Engineering, Queensland University of Technology, Brisbane, QLD, Australia

OPEN ACCESS

Edited by:

Bin Wang,
Chongqing Medical University, China

Reviewed by:

Chunqiu Zhang,
Tianjin University, China
Shaopeng Pei,
University of Pennsylvania,
United States

*Correspondence:

Qiang Chen
cq@seu.edu.cn
Xuhua Lu
xuhualu@hotmail.com

[†]These authors have contributed
equally to this work

Specialty section:

This article was submitted to
Biomechanics,
a section of the journal
Frontiers in Bioengineering and
Biotechnology

Received: 29 November 2021

Accepted: 07 February 2022

Published: 03 March 2022

Citation:

Han L, Li Y, Li Z, Ma H, Wang C,
Chen Q and Lu X (2022)
Biomechanical and Clinical Study of
Rod Curvature in Single-Segment
Posterior Lumbar Interbody Fusion.
Front. Bioeng. Biotechnol. 10:824688.
doi: 10.3389/fbioe.2022.824688

Objective: Pedicle screw fixation is a common technique used in posterior lumbar interbody fusion (PLIF) surgery for lumbar disorders. During operation, rod contouring is often subjective and not satisfactory, but only few studies focused on the rod-contouring issue previously. The aim of the study was to explore the effect of the rod contouring on the single-segment PLIF by the finite element (FE) method and retrospective study.

Methods: A FE model of the lumbosacral vertebrae was first reconstructed, and subsequently single-segmental (L4/5) PLIF surgeries with four rod curvatures (RCs) were simulated. Herein, three RCs were designed by referring to centroid, Cobb, and posterior tangent methods applied in the lumbar lordosis measurement, and zero RC indicating straight rods was included as well. Clinical data of patients subjected to L4/5 segmental PLIF were also analyzed to verify the correlation between RCs and clinical outcome.

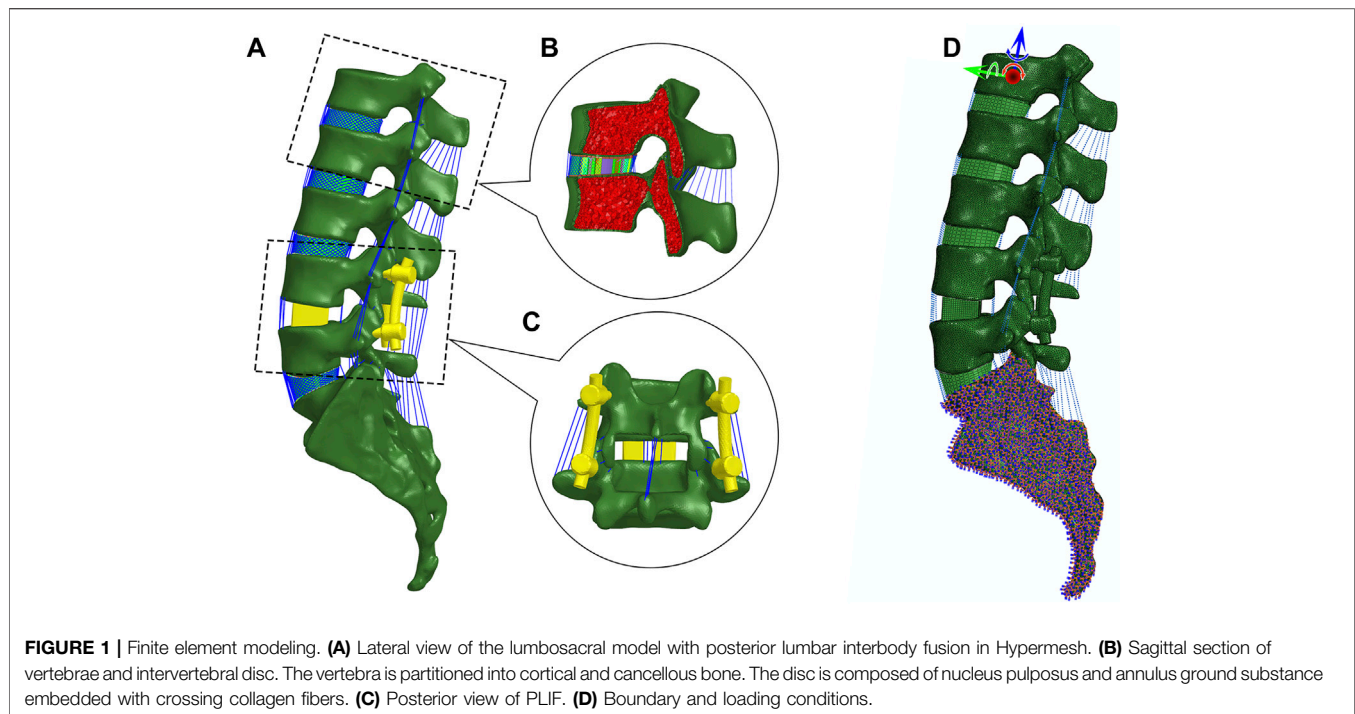
Results: No difference was observed among the four RC models in the range of motion (ROM), intersegmental rotation angle (IRA), and intradiscal pressure (IDP) under four actions. The posterior tangent model had less maximum stress in fixation (MSF) in flexion, extension, and axial rotation than the other RC models. Patients with favorable prognosis had larger RC and positive RC minus posterior tangent angle (RC-PTA) of fused segments with respect to those who had poor prognosis and received revision surgery.

Conclusion: All RC models had similar biomechanical behaviors under four actions. The posterior tangent-based RC model was superior in fixation stress distribution compared to centroid, Cobb, and straight models. The retrospective study demonstrated that moderate RC and positive RC-PTA were associated with better postoperative results.

Keywords: rod curvature, rod contouring, lumbar surgery, finite element analysis, PLIF surgery

INTRODUCTION

Optimal sagittal alignment plays a significant role in improving the spinal sagittal balance, reducing body energy expenditure, and slowing down the disc degeneration of adjacent segments (Makhni et al., 2018). Loss of the spinal sagittal balance can be caused by disc degeneration, spinal deformity, trauma, and surgery, and thus higher muscular force is required to maintain the spinal posture and balance. However,



the compensatory mechanism may result in adverse effects such as back pain, disability, and decrease in health-related quality of life (HRQOL). In addition, positive sagittal balance indicated by abnormal radiographic parameters is also highly correlated to the adverse outcomes in adult spinal deformity (Glassman et al., 2005).

Restoration of normal sagittal alignment is critical to postoperative outcomes and prognosis (Matsumoto et al., 2017). After spinal fusion, increased stress on the adjacent discs may result in adjacent segment degeneration (ASD). It was reported that the incidences of radiograph ASD and symptomatic ASD were 26.6 and 8.5% in lumbar surgery, respectively (Xia et al., 2013). Sagittal imbalance, such as sagittal vertical axis (SVA) > 50 mm, higher pelvic tilt (PT), decreased lumbar lordosis (LL), and pelvic incidence minus lumbar lordosis (PI-LL) mismatch, is identified as a significant risk factor of ASD after posterior lumbar interbody fusion (PLIF) (Barrey and Darnis, 2015). This pathological change can cause neurologic symptoms which require further medical interventions.

In view of the significance of the normal sagittal alignment, the posterior screw-rod system as the main fixation device and rod curvature (RC) should be consistent with the physiological alignment to achieve satisfactory postoperative outcomes. Otherwise, negative postoperative outcomes can be introduced. For instance, changes in the bending curvature of the implanted rod resulted in overcorrection or undercorrection of the sagittal balance in adolescent idiopathic scoliosis (Salmingo et al., 2014), and the mismatch between RC and normal sagittal alignment correlated to the poor clinical and radiological follow-up (Moufid et al., 2019).

However, perioperative rod contouring or rod bending was rarely studied previously. In clinical practice, French bender is the most commonly used tool for rod contouring. The surgeon uses the device to bend rods according to experience and preference after

evaluating the sagittal alignment of patients from the radiography during the operation. Obviously, this experience- or preference-based practice is inevitably subjective and poorly repeatable. Moreover, repetitive rod contouring is likely to cause imprecise fixation, screw loosening, stress concentration, and long operation duration. Therefore, evaluating the rod contouring indicated by RC is necessary. Herein, finite element (FE) analysis was adopted to evaluate the biomechanical effects of four RCs on the single-segment PLIF surgery including three kinds of contoured rods corresponding to three commonly used LL measuring methods (*i.e.*, centroid, Cobb, and posterior tangent) and straight rod. Then, a retrospective clinical study was conducted to discuss whether the RC was correlated with the clinical outcome.

MATERIALS AND METHODS

Finite Element Modeling

A three-dimensional FE model of the lumbar vertebrae (Figure 1) was first reconstructed through Mimics 16.0 software (Materialise, Leuven, Belgium), based on computed tomography images (CT, Philips Brilliance iCT 256; slice thickness, 1 mm; scanning voxel size, $0.8 \times 0.8 \times 1.2 \text{ mm}^3$) of a normal male adult without any lumbar disease. The participant was provided a written informed consent prior to the enrollment, and the study protocol was approved by the Institutional Ethics Committee.

Regarding the FE model, the cortical bone, cancellous bone, endplates, and intervertebral disc were created in 3-matic 8.0 (Materialise, Leuven, Belgium) and then meshed in HyperWorks 13.0 (Altair Engineering, Inc., Executive Park, CA, United States). Cortical bone was separated from each vertebra with a thickness of 1 mm (Naserkhaki et al., 2018), and the rest of the vertebra was

TABLE 1 | Material properties of the FE model.

Component	Element type	Young's modulus (Mpa)	Poisson's ratio	Density (g/cm ³)	Cross section (mm ²)	Reference				
Bone										
Cortical bone	C3D4	12,000	0.3	1.7e-6		Goel et al. (1994)				
Cancellous bone	C3D4	100	0.2	1.1e-6						
Endplate	C3D8H	23.8	0.4	1.2e-6		Ueno and Liu (1987)				
Intervertebral disc										
Annulus ground substance	C3D8H	C ₁₀ = 0.18, C ₀₁ = 0.045		1.05e-6		Schmidt et al. (2007)				
Nucleus pulpous	C3D8H	C ₁₀ = 0.12, C ₀₁ = 0.03		1.02e-6						
Annulus fiber layers										
Outermost	T3D2	550	0.3	1.0e-6	0.70	Polikeit et al. (2003)				
Second	T3D2	495	0.3	1.0e-6	0.63					
Third	T3D2	440	0.3	1.0e-6	0.55					
Fourth	T3D2	420	0.3	1.0e-6	0.49					
Fifth	T3D2	385	0.3	1.0e-6	0.41					
Innermost	T3D2	360	0.3	1.0e-6	0.30					
Fixation devices										
Screw and rod (Ti6Al4V)	C3D4	113,000	0.3							
Cage (PEEK)	C3D8H	3,500	0.3							
Ligaments	Element type	Strain (%)	Stiffness (N/mm)	Strain (%)	Stiffness (N/mm)	Strain (%)	Stiffness (N/mm)	Strain (%)	Stiffness (N/mm)	Reference
Anterior longitudinal ligament	Spring A	$\epsilon < 0$	0	$0 < \epsilon < 12.2$	347	$12.2 < \epsilon < 20.3$	787	$20.3 < \epsilon$	1864	Rohlmann et al. (2006)
Posterior longitudinal ligament	Spring A			$0 < \epsilon < 11.1$	29.5	$11.1 < \epsilon < 23$	61.7	$23 < \epsilon$	236	
Ligamentum flavum	Spring A			$0 < \epsilon < 5.9$	7.7	$5.9 < \epsilon < 49$	9.6	$49 < \epsilon$	58.2	
Intertransverse ligament	Spring A			$0 < \epsilon < 18.2$	0.3	$18.2 < \epsilon < 23.3$	1.8	$23.3 < \epsilon$	10.7	
Capsular ligament	Spring A			$0 < \epsilon < 25$	36	$25 < \epsilon < 30$	159	$30 < \epsilon$	384	
Interspinous ligament	Spring A			$0 < \epsilon < 13.9$	1.4	$13.9 < \epsilon < 20$	1.5	$20 < \epsilon$	14.7	
Supraspinous ligament	Spring A			$0 < \epsilon < 20$	2.5	$20 < \epsilon < 25$	5.3	$25 < \epsilon$	34	

treated as cancellous bone. The thickness of the endplate was set at 0.5 mm. The element types of vertebrae and endplates were four-node tetrahedral element (C3D4) and eight-node hybrid hexahedral elements (C3D8H), respectively. Intervertebral discs were divided into incompressible nucleus pulposus and annulus ground substance (Guo and Fan, 2018). The nucleus pulposus and annular ground substance were meshed by the C3D8H element with an isotropic, hyper-elastic Mooney–Rivlin material. Six circumferential layers of crossing collagen fibers with different orientations were embedded in the annulus ground substance, and the fibers were meshed by tension-only two-node truss elements (T3D2). A total of seven major ligaments including anterior longitudinal ligament (ALL), posterior longitudinal ligament (PLL), ligamentum flavum (LF),

capsular ligament (CL), intertransverse ligament (ITL), interspinous ligament (ISL), and supraspinous ligament (SSL) were meshed by tension-only Spring A elements (Rohlmann et al., 2006). A frictionless surface contact between facet joints was assigned. All material properties of the aforementioned tissues were listed in Table 1.

Contouring Methods and Simulation of the Posterior Lumbar Interbody Fusion Procedure

Centroid, Cobb, and posterior tangent methods (Figure 2) were applied to measure angles of L4–L5 segment curvatures in

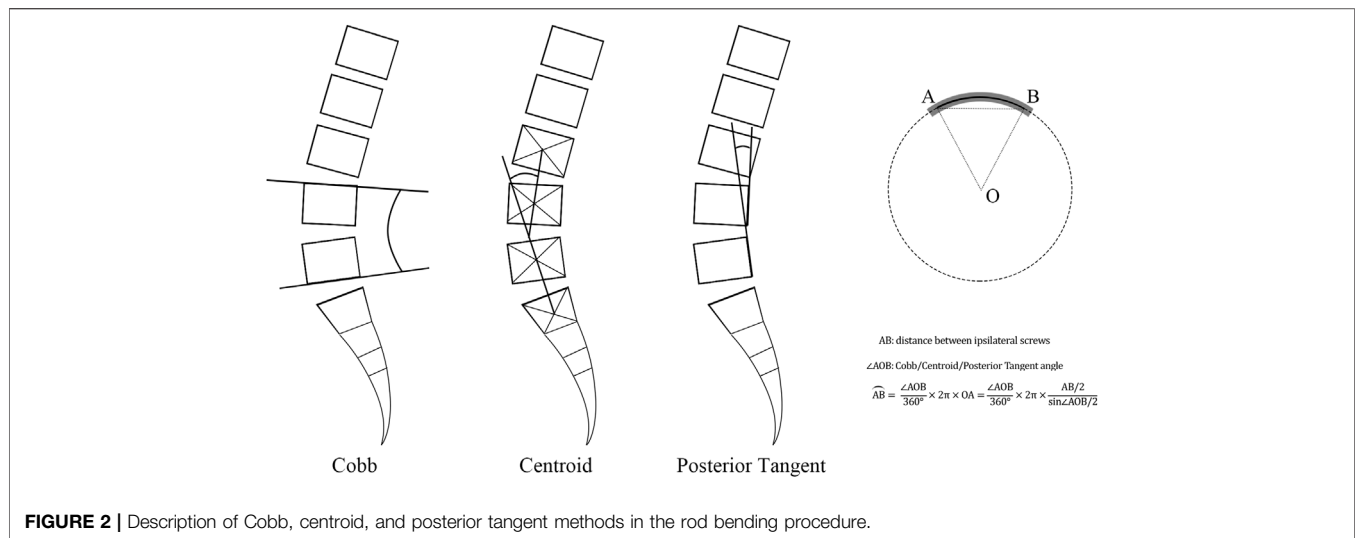


FIGURE 2 | Description of Cobb, centroid, and posterior tangent methods in the rod bending procedure.

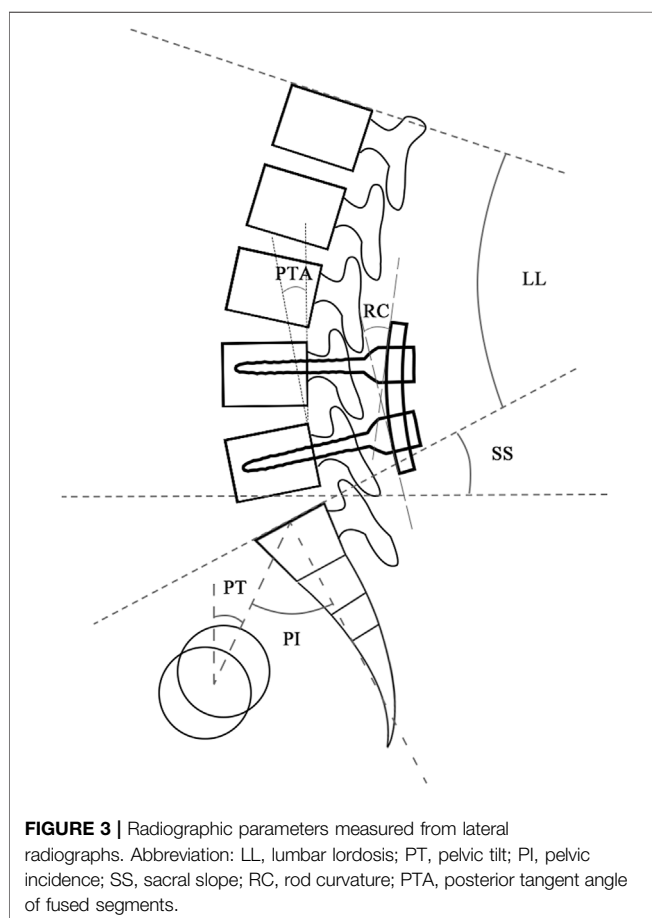


FIGURE 3 | Radiographic parameters measured from lateral radiographs. Abbreviation: LL, lumbar lordosis; PT, pelvic tilt; PI, pelvic incidence; SS, sacral slope; RC, rod curvature; PTA, posterior tangent angle of fused segments.

Mimics (Harrison et al., 2001). Here, the centroid angle was described as the included angle made by two straight lines, which passed through two vertebral centroids at both ends (Chen, 1999). The Cobb angle was defined as the angle between the superior endplate of L4 and the inferior endplate of L5. The posterior

tangent angle was defined as the included angle of two lines passing tangentially to posterior wall of the L4 and L5 end vertebrae (Janik et al., 1998). The shape of the contoured rod was simply treated as an arc of a virtual circle. According to the distance between ipsilateral screw tails (*i.e.*, chord length of the arc) and the three previously defined angles, the arc length (*i.e.*, the rod contour) was calculated. The RCs of centroid, Cobb, and posterior tangent models were 33.25°, 18.65°, and 7.99°, respectively. In addition, the straight model (RC = 0°) was also considered. Accordingly, the four types of rods were modeled in SolidWorks 2003 (SolidWorks Corp., Waltham, MA, United States).

PLIF was modeled on L4–L5 segment in 3-matic software. According to the surgical procedure, pedicle screws with a diameter of 6 mm were inserted along the central axis of the pedicle, and two screws in L4 and L5 were parallel to their superior endplates, respectively. Partial spinous processes and laminae (inferior L4 and superior L5) and half of the medial facet joints and three ligaments (LF, ISL, and SSL between L4 and L5) were removed. Then, two cubic cages were inserted into the disc space after removing the inferior endplate of L4 and superior endplate of L5, and this simulated the clinical practice. Finally, rods with four RCs were assembled in each model. All fixation devices were meshed in HyperWorks. Tie constraints were employed to model the contact between vertebrae and screws or cages. All material properties of fixation devices were also reported in **Table 1**.

Boundary and Loading Conditions

The six degrees-of-freedom of the sacrum were constrained. The loading history involved two steps. In the first step, a preload of 500 N as a follower load representing upper body weight and muscle forces was applied according to the force line of the lumbar spine (Patwardhan et al., 1999). In the second step, a 7.5 N m moment was applied on the top center of the L1 vertebral body in four actions, *i.e.*, flexion, extension, lateral bending, and axial rotation (Ayturk and Puttllitz, 2011). FE simulation was

performed by Abaqus (v6.14, Simulia Inc., Providence, RI, United States).

Model Validation and FE Analysis

To validate the FE model, a normal lumbosacral model was also developed (Supplementary Figure S1 in Supplementary Materials), and the range of motion (ROM) of the normal lumbosacral model and L4/5 intradiscal pressure (IDP) were compared with a recent FE study and an *in vitro* biomechanical experiment (Rohlmann et al., 2001; Wang et al., 2018). To be consistent with the literature, a follower load of 280 N and increasing moments from 0.0 to 7.5 N m with an interval 2.5 N m were applied on the FE model in flexion, extension, lateral bending, and axial rotation tests. After the validation, ROM, intersegmental rotation angle (IRA) of adjacent levels, IDP in adjacent segmental discs, and maximum von Mises stress in fixation (MSF) of the four RC models were compared (Huang et al., 2021).

Clinical Study

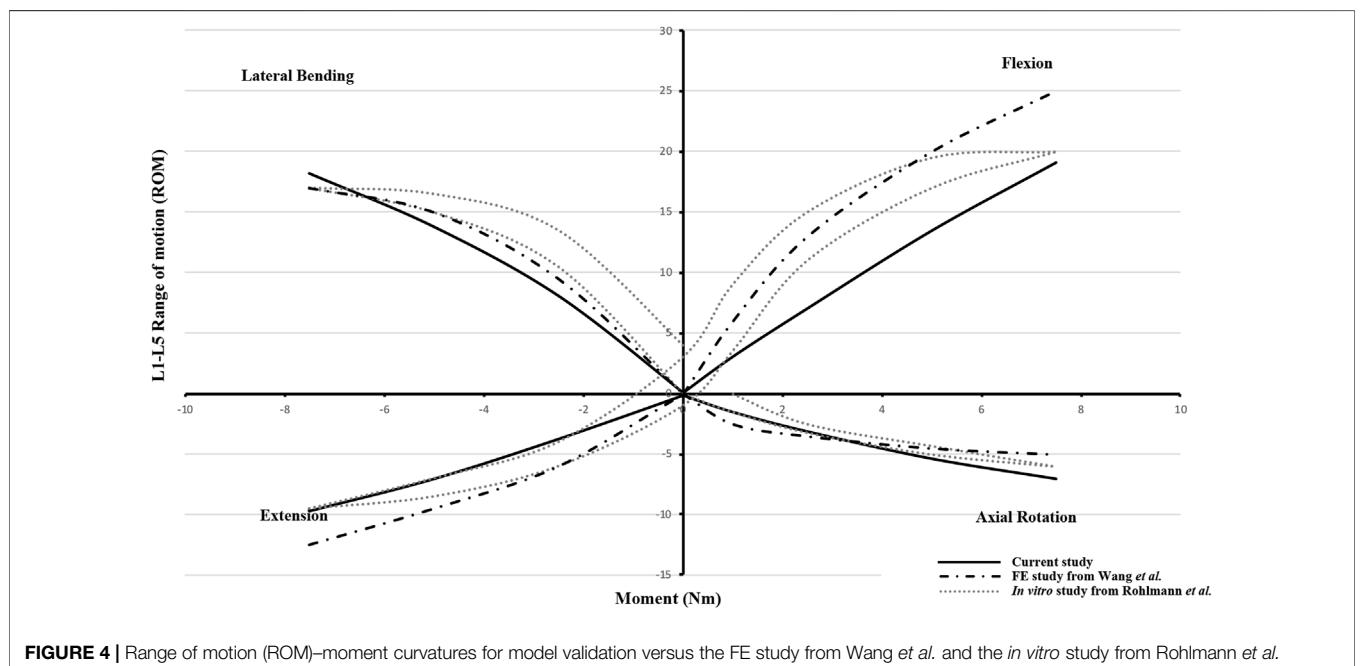
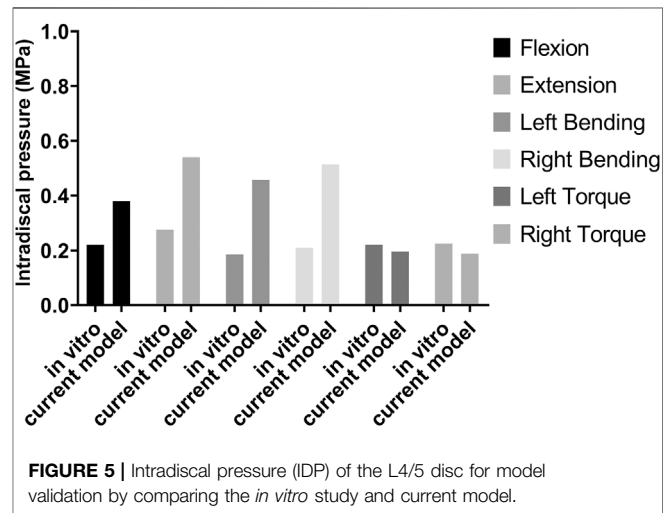
The retrospective study identified patients subjected to L4/5 segmental PLIF surgery for lumbar spinal stenosis from January 2015 to June 2021 with the Institutional Review Board’s (IRB) approval. The exclusion criteria were patients with the diagnosis of spinal infection, injury, tumor, apparent deformity, irreducible lumbar spondylolisthesis, and other diseases that caused spinal instability. The normal group included patients with an over two-year satisfactory follow-up, whereas the abnormal group consisted of patients who had poor recovery within two-year follow-up after primary surgery and received revision surgery. Patient demographics (age, gender, and BMI), surgical time, and hospital stay were collected. Radiographic parameters including LL, PT, PI, sacral slope (SS), PI-LL, RC, posterior tangent angle of fused segments

(PTA), and the difference between RC and PTA (RC-PTA) were measured from postoperative lateral radiographs (Figure 3). The χ^2 test for the parameter of gender and student *t*-test for the remaining parameters were used to determine statistical difference between groups (SPSS Statistics 16.0, IBM Corporation, Somers, NY, United States), and $p < 0.05$ indicated the statistical significance.

RESULTS

Model Validation

The ROM of the normal lumbosacral model was validated against two previous studies (Rohlmann et al., 2001; Wang et al., 2018).



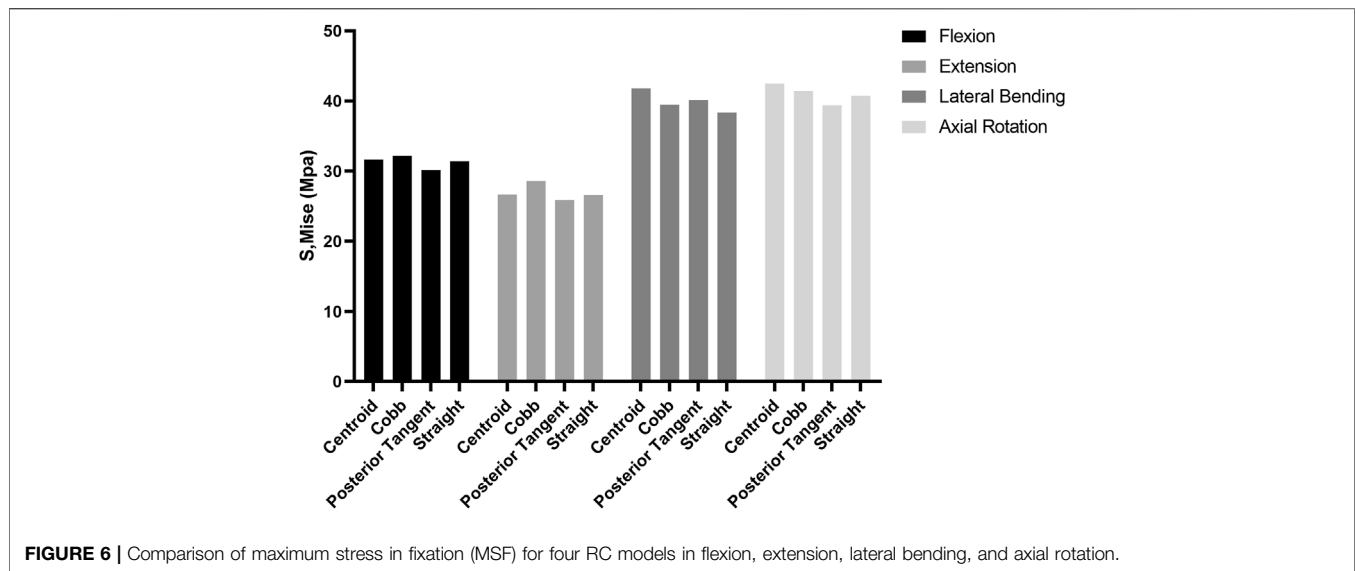


FIGURE 6 | Comparison of maximum stress in fixation (MSF) for four RC models in flexion, extension, lateral bending, and axial rotation.

As shown in **Figure 4**, the ROM–moment curves in the current study agree with the ranges of the *in vitro* study and FE study. The distribution of the IDP in L4/5 is similar to that of the *in vitro* study, *i.e.*, extension > right bending > left bending > flexion > left torque > right torque. However, compared to the axial torsion, the IDPs of flexion, extension, and lateral bending between the present FE result and the *in vitro* experiment show a discrepancy (**Figure 5**). The reason might be that residual muscles or tendons connecting the spine in the *in vitro* study reduced the stress level of the IDP. In any case, IDPs in the current study are still in the acceptable ranges (Dreischarf et al., 2014; Naserkhaki et al., 2018).

Biomechanical Analysis of the Groups

No difference in the ROM of the lumbosacral model in the single-segmental PLIF surgery was observed among four RC models under the four actions of flexion, extension, lateral bending, and axial rotation (**Supplementary Figure S2** in Supplementary Materials). On the neighboring adjacent vertebrae (L3/4 and L5/S1) to the fused L4/5, there was also no substantial difference among four RC models in IRA and IDP with 7.5 N m moment under the four actions (**Supplementary Figure S3** in Supplementary Materials). Stress distributions of the intervertebral discs and vertebrae showed a very weak difference between four RC models (**Supplementary Figures S4, S5** in Supplementary Materials). The stress levels of collagen fibers were higher than those of annulus ground substance. In particular, MSFs under the four actions are illustrated in **Figure 6**. In flexion and extension, the Cobb model had the greatest stress, followed by the centroid model, straight model, and finally posterior tangent model. In the lateral bending and axial rotation, the greatest maximum stresses occurred in the centroid model; however, the posterior tangent model and Cobb model ranked the second and third, respectively, and the straight model was the last in the lateral bending, whereas in axial rotation, Cobb and straight models were in the middle, and posterior tangent had the minimum stress. The stress contours of the screw–rod system in four RC models with the values and locations of MSF under the four actions are shown in **Figure 7**. Overall, MSF in all RC models mainly occurred at the

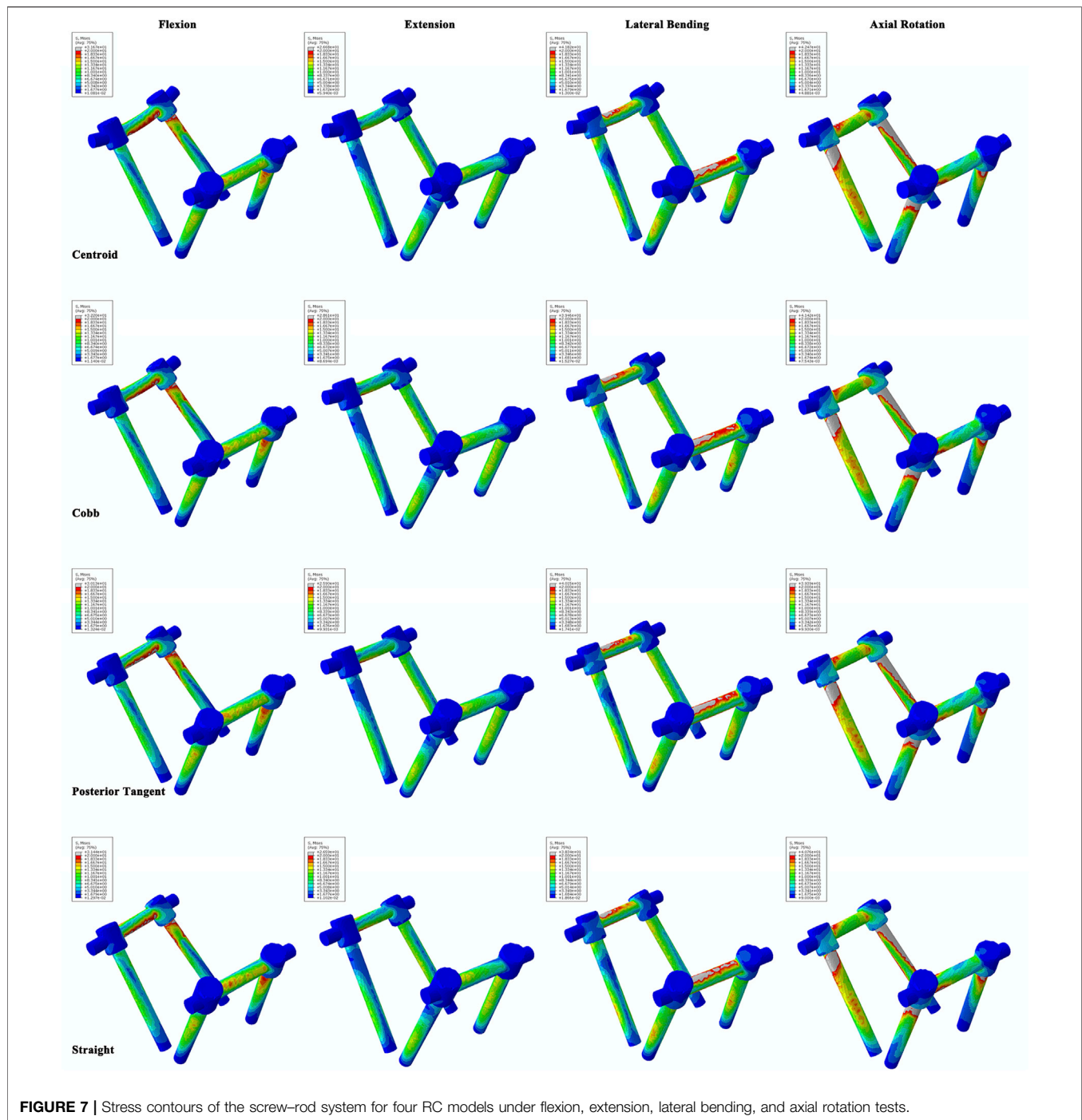
junction of screw and rods, and stress concentration was located at rods and thread run-out. In axial rotation, the screw–rod system experienced larger stress concentration than other actions.

Clinical Results

The analysis for characteristics of patients undergoing L4/5 segmental PLIF surgery were listed in **Table 2**. The primary diagnoses for reoperations were lumbar spinal stenosis at the adjacent level (10 cases) and internal fixation failure (2 cases). No significant differences were found between normal and abnormal groups in aspects of age, gender, BMI, surgical time, hospital stay, LL, PT, PI, SS, PI-LL, and PTA. The normal group had much higher RC (18.87° versus 4.70°, $p < 0.01$) and RC-PTA (6.18° versus -5.23°, $p < 0.01$) than the abnormal group (**Figure 8**).

DISCUSSION

Optimization of spinal alignment measurements could provide guidance to the surgery. However, one question that needs to be answered is whether the rod contouring process should follow the same strategy. In the process of sagittal alignment correction, there is no evaluation on what RC could achieve a better clinical outcome. Thus, basing on three commonly-used LL measurements, we applied an analogy to rod contouring practice in spinal surgery and provided evidence for better rod contouring in single-segmental PLIF surgery by FE simulation. Although the three methods showed similar biomechanical properties under four actions, the posterior tangent method was relevantly superior in the fixation stress distributions of flexion, extension, and axial rotation. The RCs in centroid, Cobb, posterior tangent, and straight models were 33.25°, 18.65°, 7.99°, and 0°. Also, the RC-PTA of the four models were 25.26°, 10.66°, 0°, and -7.99°, respectively. The two variables of the posterior tangent model fell in the middle of the ranges. In the clinical study, it was demonstrated that moderate RC was beneficial for patients who underwent L4/5



segmental PLIF surgery, and negative RC-PTA was associated with adverse postoperative outcomes. Hence, both FEA and clinical study demonstrated that moderate rod contouring was necessary in L4/5 PLIF surgery. This result was partially consistent with Harrison's finding with respect to algorithm comparison of LL assessment (Harrison et al., 2001). Combined with the analyzing methodologies, the posterior tangent method seemed better to fit normal spinal cord. Thus, we inferred that for the sake of convenience in clinical

application, employing the fitting curve of the normal lumbar vertebral posterior edge or centerline of spinal canal to contour rod could be a feasible approach.

To date, improvement of surgical outcome and prevention of ASD-related complications are still the focus and challenge in lumbar surgery. In clinical practice, disappointing postoperative function and mechanical failure have been largely ascribed to inadequate restoration of sagittal alignment. Appropriate LL restoration was beneficial for reducing ASD risk. An *in vitro*

TABLE 2 | Patient demographics and radiographic parameters.

Variable	Normal (N = 19)	Revision (N = 12)	p-value
Age (years)	53.42 ± 10.05	52.71(0.15)	0.42
Gender (male/female)	10/9	9/3	0.27
BMI (kg/m ²)	25.59 ± 3.32	23.49 ± 2.93	0.08
Surgical time (hour)	2.21 ± 0.38	2.46 ± 0.99	0.47
Hospital stay (days)	7.74 ± 3.33	6.67 ± 1.83	0.32
LL	52.62 ± 12.30	48.49 ± 7.97	0.31
PT	15.12 ± 6.95	18.79 ± 4.26	0.11
PI	51.12 ± 6.95	52.74 ± 8.67	0.67
SS	35.99 ± 7.52	33.95 ± 7.90	0.48
PI-LL	-1.51 ± 10.19	4.25 ± 7.84	0.11
RC	18.87 ± 6.16	4.70 ± 3.39	<0.01
PTA	12.68 ± 5.05	9.93 ± 3.09	0.10
RC-PTA	6.18 ± 7.96	-5.23 ± 4.71	<0.01

Abbreviation: LL, lumbar lordosis; PT, pelvic tilt; PI, pelvic incidence; SS, sacral slope; PI-LL, the difference between PI and LL; RC, rod curvature; PTA, posterior tangent angle of fused segments; RC-PTA, the difference between RC and PTA.

biomechanical study reported that hypolordosis in the fused segments could reduce tension behavior of the anterior soft tissues and increase the stress of the posterior column of the adjacent vertebra (Umehara et al., 2000). Meanwhile, high stress of posterior internal fixation might increase risks of screw loosening or rupture. Moreover, decreased LL could increase the ROM and IDP of adjacent segments (Zhao et al., 2018), and excessive LL curvature also increased the IDP of the adjacent intervertebral disc (Wang et al., 2020). These also indicate the potential risk of ASD

development. A meta-analysis revealed that post-operative LL was correlated with a significant increase in ASD occurrence after PLIF for degenerative lumbar disease (Wang and Ding, 2020). In this regard, to maintain proper physiologic lordosis at the fusion site, RC should be in accordance with the appropriate LL. This inference supplies the theoretical support for the current study to some extent. In addition, it must be pointed out that proper physiologic lordosis cannot be equated with originally normal lumbar alignment for degenerative lumbar disease. Vertebral osteophyte formation, intervertebral disc degeneration, facet hypertrophy, and compensatory change of surrounding tissues are the reflections of the body's restabilization dealing with the lumbar pathological state in a long-term process. This spontaneous restabilization generates a special biomechanical status distinct from a patient's normal lumbar condition or individuals with normal anatomic structure of lumbar spine. Thus, it requires proper correction of lumbar curvature based on clinical patient-specific conditions, and this challenges surgeons when evaluating spinal balance and planning correction of curvature.

To the best knowledge of the authors, there are few studies on the rod contouring optimization. Wanivenhaus et al. (2019) proposed that augmented reality-assisted rod bending could reduce operation duration by 20% compared with the traditional method and achieve higher accuracy of the rod bending process. Shi et al. (2020) confirmed that the Cobb angle could be used as reference to guide rod bending in thoracolumbar fractures and also reported that 4°–8° greater than the Cobb angle as the RC achieved the best spinal sagittal balance 2 years after the operation. Moufid et al.

**FIGURE 8** | Typical cases showing rod contouring differences between normal and abnormal groups.

(2019) evaluated the mismatch between rod–screw and LL of the fused segment by the concept of the mismatch analysis index (MAI), which was determined by three parameters: the angle between the screw and rod, the angle between the superior endplate and screw, and the distance between the rod and posterior wall of vertebra. In addition, Wang et al. (2016) reported that increasing the bending angle of the concave rod, with respect to the convex rod, could improve the transverse plane correction with advantages in screw pullout forces and kyphosis.

The present study has a certain significance in the practical application of individualized or customized rod contouring before operation. Precise contouring could avoid the reduction of yield strength and stiffness caused by repetitive bending (Demura et al., 2015). It is worth noting that this study made a preliminary exploration on a habitual, pervasive, but subjective surgical procedure that requires standardization in the period of highly developing surgical techniques. Limitations should be acknowledged as well. First, this study did not take into account anatomical variations of the spinal structure. In fact, normal lumbar curvature varies greatly, which may result in different biomechanical performances of rod contouring. Spinal parameters, such as LL, PI, PT, and sacral slope (SS), are also associated with the sagittal balance. Second, the current study computationally modeled three commonly used lumbar lordosis measurements and straight rods to guide rod contouring. However, the modeled RCs should be solidified to have generalizability, interpretability, and clinical applicability by collecting more samples. Third, the clinical observations were patient-specific, and the real mechanical environment corresponding to the model boundary conditions varied, and this might lead to the discrepancy between the model and clinical observations. The patient-specific information should be further included to have exactly consistent results with the clinical observations. Fourth, FEA was a numerical evaluation of the biomechanical effect on the PLIF. The cadaveric study under cyclic loading and multicenter clinical studies with sound evidence should be conducted to verify the results. The accuracy of the radiographic parameter measurement could also be optimized by digital image processing and other analysis techniques. Nevertheless, there is no denying that the current study strongly controlled variables that inevitably occurred in clinical studies such as differences from patients and fixation placement.

CONCLUSION

The present study studied the biomechanical effects of different RCs determined by centroid, Cobb, and posterior tangent

REFERENCES

- Ayturk, U. M., and Puttlitz, C. M. (2011). Parametric Convergence Sensitivity and Validation of a Finite Element Model of the Human Lumbar Spine. *Comput. Methods Biomech. Biomed. Eng.* 14 (8), 695–705. doi:10.1080/10255842.2010.493517
- Barrey, C., and Darnis, A. (2015). Current Strategies for the Restoration of Adequate Lordosis during Lumbar Fusion. *World J. Orthop.* 6 (1), 117–126. doi:10.5312/wjo.v6.i1.117
- Chen, Y.-L. (1999). Vertebral Centroid Measurement of Lumbar Lordosis Compared with the Cobb Technique. *Spine (Phila Pa 1976)* 24 (17), 1786–1790. doi:10.1097/00007632-199909010-00007
- Demura, S., Murakami, H., Hayashi, H., Kato, S., Yoshioka, K., Yokogawa, N., et al. (2015). Influence of Rod Contouring on Rod Strength and Stiffness in Spine Surgery. *Orthopedics* 38 (6), e520–523. doi:10.3928/01477447-20150603-61
- Dreischarf, M., Zander, T., Shirazi-Adl, A., Puttlitz, C. M., Adam, C. J., Chen, C. S., et al. (2014). Comparison of Eight Published Static Finite Element Models of the Intact Lumbar Spine: Predictive Power of Models Improves when Combined Together. *J. Biomech.* 47 (8), 1757–1766. doi:10.1016/j.jbiomech.2014.04.002

methods on the single-segment PLIF surgery. The findings were that four RC models showed similar biomechanical behaviors under four actions, but the posterior tangent mode was relevantly superior to other three RC models in the aspect of fixation stress distribution. Moreover, the retrospective study further revealed that moderate RC and positive RC-PTA were associated with favorable prognosis.

DATA AVAILABILITY STATEMENT

The original contributions presented in the study are included in the article/**Supplementary Material**, further inquiries can be directed to the corresponding authors.

ETHICS STATEMENT

The studies involving human participants were reviewed and approved by Medical Ethics Committee of Shanghai Changzheng Hospital. The patients/participants provided their written informed consent to participate in this study.

AUTHOR CONTRIBUTIONS

LH and XL designed the research. LH and YL conducted the study. ZL, HM, and CW performed data collection and analysis. LH wrote the draft of this manuscript. QC, ZL, and XL revised the article critically. QC and XL were the guarantors.

FUNDING

This study was supported by the Pyramid Talent Project (No. 0910) and the Project of Shanghai Science and Technology Committee (No. 19140901400), and was partially supported by the National Natural Science Foundation of China (No. 32171307).

SUPPLEMENTARY MATERIAL

The Supplementary Material for this article can be found online at: <https://www.frontiersin.org/articles/10.3389/fbioe.2022.824688/full#supplementary-material>

- Glassman, S. D., Berven, S., Bridwell, K., Horton, W., and Dimar, J. R. (2005). Correlation of Radiographic Parameters and Clinical Symptoms in Adult Scoliosis. *Spine (Phila Pa 1976)* 30 (6), 682–688. doi:10.1097/01.brs.0000155425.04536.f7
- Goel, V. K., Park, H., and Kong, W. (1994). Investigation of Vibration Characteristics of the Ligamentous Lumbar Spine Using the Finite Element Approach. *J. Biomech. Eng.* 116 (4), 377–383. doi:10.1115/1.2895787
- Guo, L.-X., and Fan, W. (2018). Dynamic Response of the Lumbar Spine to Whole-Body Vibration under a Compressive Follower Preload. *Spine (Phila Pa 1976)* 43 (3), E143–E153. doi:10.1097/BRS.0000000000002247
- Harrison, D. E., Harrison, D. D., Cailliet, R., Janik, T. J., and Holland, B. (2001). Radiographic Analysis of Lumbar Lordosis: Centroid, Cobb, TRALL, and Harrison Posterior tangent Methods. *Spine (Phila Pa 1976)* 26 (11), E235–E242. doi:10.1097/00007632-200106010-00003
- Huang, H., Liu, J., Wang, L., and Fan, Y. (2021). A Critical Review on the Biomechanical Study of Cervical Interbody Fusion Cage. *Med. Novel Technol. Devices* 11, 100070. doi:10.1016/j.medntd.2021.100070
- Janik, T. J., Harrison, D. D., Cailliet, R., Troyanovich, S. J., and Harrison, D. E. (1998). Can the Sagittal Lumbar Curvature Be Closely Approximated by an Ellipse? *J. Orthop. Res.* 16 (6), 766–770. doi:10.1002/jor.1100160620
- Makhni, M. C., Shillingford, J. N., Laratta, J. L., Hyun, S.-J., and Kim, Y. J. (2018). Restoration of Sagittal Balance in Spinal Deformity Surgery. *J. Korean Neurosurg. Soc.* 61 (2), 167–179. doi:10.3340/jkns.2017.0404.013
- Matsumoto, T., Okuda, S., Maeno, T., Yamashita, T., Yamasaki, R., Sugiura, T., et al. (2017). Spinopelvic Sagittal Imbalance as a Risk Factor for Adjacent-Segment Disease after Single-Segment Posterior Lumbar Interbody Fusion. *J. Neurosurg. Spine* 26 (4), 435–440. doi:10.3171/2016.9.SPINE16232
- Moufid, A. Y., Cloche, T., Ghailane, S., Ounajim, A., Vendeuvre, T., and Gille, O. (2019). Mismatch between Rod Bending and Actual Post-Operative Lordosis in Lumbar Arthrodesis with Poly Axial Screws. *Orthop. Traumatol. Surg. Res.* 105 (6), 1143–1148. doi:10.1016/j.otsr.2019.03.003
- Naserkhaki, S., Arjmand, N., Shirazi-Adl, A., Farahmand, F., and El-Rich, M. (2018). Effects of Eight Different Ligament Property Datasets on Biomechanics of a Lumbar L4-L5 Finite Element Model. *J. Biomech.* 70, 33–42. doi:10.1016/j.jbiomech.2017.05.003
- Patwardhan, A. G., Havey, R. M., Meade, K. P., Lee, B., and Dunlap, B. (1999). A Follower Load Increases the Load-Carrying Capacity of the Lumbar Spine in Compression. *Spine (Phila Pa 1976)* 24 (10), 1003–1009. doi:10.1097/00007632-199905150-00014
- Polikeit, A., Ferguson, S. J., Nolte, L. P., and Orr, T. E. (2003). Factors Influencing Stresses in the Lumbar Spine After the Insertion of Intervertebral Cages: Finite Element Analysis. *Eur. Spine J.* 12 (4), 413–420. doi:10.1007/s00586-002-0505-8
- Rohlmann, A., Bauer, L., Zander, T., Bergmann, G., and Wilke, H.-J. (2006). Determination of Trunk Muscle Forces for Flexion and Extension by Using a Validated Finite Element Model of the Lumbar Spine and Measured *In Vivo* Data. *J. Biomech.* 39 (6), 981–989. doi:10.1016/j.jbiomech.2005.02.019
- Rohlmann, A., Neller, S., Claes, L., Bergmann, G., and Wilke, H.-J. (2001). Influence of a Follower Load on Intradiscal Pressure and Intersegmental Rotation of the Lumbar Spine. *Spine (Phila Pa 1976)* 26 (24), E557–E561. doi:10.1097/00007632-200112150-00014
- Salmingo, R. A., Tadano, S., Abe, Y., and Ito, M. (2014). Influence of Implant Rod Curvature on Sagittal Correction of Scoliosis Deformity. *Spine J.* 14 (8), 1432–1439. doi:10.1016/j.spinee.2013.08.042
- Schmidt, H., Heuer, F., Drumm, J., Klezl, Z., Claes, L., and Wilke, H. J. (2007). Application of a Calibration Method Provides More Realistic Results for a Finite Element Model of a Lumbar Spinal Segment. *Clin Biomech.* 22 (4), 377–384. doi:10.1016/j.clinbiomech.2006.11.008
- Shi, Z., Wang, G., Jin, Z., Wu, T., Wang, H., Sun, J., et al. (2020). Use of the Sagittal Cobb* Angle to Guide the Rod Bending in the Treatment of Thoracolumbar Fractures: A Retrospective Clinical Study. *J. Orthop. Surg. Res.* 15 (1), 574. doi:10.1186/s13018-020-02115-5
- Ueno, K., and Liu, Y. K. (1987). A Three-Dimensional Nonlinear Finite Element Model of Lumbar Intervertebral Joint in Torsion. *J. Biomech. Eng.* 109 (3), 200–209. doi:10.1115/1.3138670
- Umehara, S., Zindrick, M. R., Patwardhan, A. G., Havey, R. M., Vrbos, L. A., Knight, G. W., et al. (20001976). The Biomechanical Effect of Postoperative Hypolordosis in Instrumented Lumbar Fusion on Instrumented and Adjacent Spinal Segments. *Spine* 25 (13), 1617–1624. doi:10.1097/00007632-200007010-00004
- Wang, K., Jiang, C., Wang, L., Wang, H., and Niu, W. (2018). The Biomechanical Influence of Anterior Vertebral Body Osteophytes on the Lumbar Spine: A Finite Element Study. *Spine J.* 18 (12), 2288–2296. doi:10.1016/j.spinee.2018.07.001
- Wang, T., and Ding, W. (2020). Risk Factors for Adjacent Segment Degeneration after Posterior Lumbar Fusion Surgery in Treatment for Degenerative Lumbar Disorders: A Meta-Analysis. *J. Orthop. Surg. Res.* 15 (1), 582. doi:10.1186/s13018-020-02032-7
- Wang, W., Pei, B., Pei, Y., Li, H., Lu, S., Wu, X., et al. (2020). Biomechanical Effects of over Lordotic Curvature after Spinal Fusion on Adjacent Intervertebral Discs under Continuous Compressive Load. *Clin. Biomech.* 73, 149–156. doi:10.1016/j.clinbiomech.2020.01.002
- Wang, X., Boyer, L., Le Naveaux, F., Schwend, R. M., and Aubin, C.-E. (2016). How Does Differential Rod Contouring Contribute to 3-dimensional Correction and Affect the Bone-Screw Forces in Adolescent Idiopathic Scoliosis Instrumentation? *Clin. Biomech.* 39, 115–121. doi:10.1016/j.clinbiomech.2016.10.002
- Wanivenhaus, F., Neuhaus, C., Liebmann, F., Roner, S., Spirig, J. M., and Farshad, M. (2019). Augmented Reality-Assisted Rod Bending in Spinal Surgery. *Spine J.* 19 (10), 1687–1689. doi:10.1016/j.spinee.2019.06.019
- Xia, X.-P., Chen, H.-L., and Cheng, H.-B. (2013). Prevalence of Adjacent Segment Degeneration after Spine Surgery. *Spine* 38 (7), 597–608. doi:10.1097/BRS.0b013e318273a2ea
- Zhao, X., Du, L., Xie, Y., and Zhao, J. (2018). Effect of Lumbar Lordosis on the Adjacent Segment in Transforaminal Lumbar Interbody Fusion: a Finite Element Analysis. *World Neurosurg.* 114, e114–e120. doi:10.1016/j.wneu.2018.02.073

Conflict of Interest: The authors declare that the research was conducted in the absence of any commercial or financial relationships that could be construed as a potential conflict of interest.

Publisher's Note: All claims expressed in this article are solely those of the authors and do not necessarily represent those of their affiliated organizations, or those of the publisher, the editors, and the reviewers. Any product that may be evaluated in this article, or claim that may be made by its manufacturer, is not guaranteed or endorsed by the publisher.

Copyright © 2022 Han, Li, Li, Ma, Wang, Chen and Lu. This is an open-access article distributed under the terms of the Creative Commons Attribution License (CC BY). The use, distribution or reproduction in other forums is permitted, provided the original author(s) and the copyright owner(s) are credited and that the original publication in this journal is cited, in accordance with accepted academic practice. No use, distribution or reproduction is permitted which does not comply with these terms.